Composite Structures 278 (2021) 114687

Contents lists available at ScienceDirect

Composite Structures

journal homepage: www.elsevier.com/locate/compstruct

Numerical design of rotationally molded composite tie rods

Jonas Nieschlag *, Philipp Eisenhardt, Sven Coutandin, Jürgen Fleischer

wbk Institute of Production Science, Karlsruhe Institute of Technology, Kaiserstr.12, 76131 Karlsruhe, Germany

ARTICLE INFO

Keywords:
Hybrid
Finite element analysis (FEA)
Mechanical testing
Rotational molding

ABSTRACT

Rotational molding constitutes a promising manufacturing technology for rotationally symmetric components made of thermoset matrix with continuous fiber reinforcement. The present study deals with the numerical analysis of a rotationally molded composite tie rod with metallic load introduction elements. For this purpose, the adhesive joint between carbon fiber reinforced plastic and metallic load introduction element was investigated in more detail. Different geometries of a spew fillet were evaluated to reduce the stress peaks occurring at the ends of the overlap. A design of experiments was used to determine the influence of the different parameters. An optimized geometry was derived and compared with a reference in terms of stress distribution. Subsequently, test specimens were rotationally molded and mechanically tested. The results of the study show that the maximum stresses within the adhesive layer can be reduced with an optimized spew fillet, and thus a higher mechanical tensile load of the composite tie rod can be achieved.

1. Introduction

Tie rods and drive shafts are used in many technical applications to transmit forces and torques, for example as actuators for landing flaps in aircraft applications or drive shafts in automotive applications. Compared to conventional metal components, the use of carbon fiber reinforced plastic (CFRP) can increase the strength and stiffness of the component while reducing its weight. In the case of a tie rod, the energy consumption of a moving system can be reduced, and the payload increased [1]. With a CFRP drive shaft, a higher bending-critical rotational speed can be achieved due to the higher specific stiffness [2]. These components are often part of a larger structure made of a metallic material. For this reason, the components are generally designed with a cylindrical body made of CFRP and metallic load introduction elements, which are connected to the rest of the bodywork.

Established processes for manufacturing profiled components using CFRP are winding, pultrusion, resin transfer molding and blow molding [3]. An alternative to these established manufacturing processes constitutes in the rotational molding process with continuous fiber reinforcement [4]. In the process variant with a thermoset matrix, a preform made of semi-finished products is placed in a mold and impregnated under rotation as shown in Fig. 1 [5,6]. The impregnation pressure is generated by the resulting centrifugal force. Once the matrix has cured, the rotational molding process can be stopped, and the finished part is removed. A major advantage compared to established manufacturing methods lies in the fact that metallic load introduction elements can be intrinsically joined in the process, without requiring any subsequent joining steps [6]. The connection can either be a co-cured joint or form-fit joint [7,8], whereby the co-cured joint is based on the adhesive properties of the matrix used. Since the length of the impregnation path is identical to the component thickness, the preform can be fully impregnated and cured in a very short time if low-viscosity matrix systems are used and sufficient heat is applied. Compared to known manufacturing processes, the rotational molding process does not require cores or expensive consumables. Merely a mold and a spindle are needed, resulting in relatively low overall investment costs for this process. For these reasons, it seems worthwhile to conduct a more in-depth scientific study of the process. The co-cured joint can be compared with a conventional adhesive bond. Accordingly, the strength of the co-cured joint depends on various factors [9]. These include:

- Thickness of the adhesive layer
- Stiffness of the adherends
- Length and width of the overlap surface
- Wetting of the joining surfaces
- Roughness of the adherends
- Geometry of the joint

Factors such as the thickness of the adhesive layer cannot be influenced during rotational molding. An increase in the stiffness of the adherends or the enlargement of the overlapping area have a negative effect on the total weight of the joint. When additional heat is applied, the viscosity of the matrix is reduced, which leads to an improved surface wetting [10]. Various surface treatments have proven beneficial

* Corresponding author.
E-mail address: jonas.nieschlag@kit.edu (J. Nieschlag).

https://doi.org/10.1016/j.compstruct.2021.114687
Received 25 May 2021; Received in revised form 30 August 2021; Accepted 11 September 2021
Available online 16 September 2021

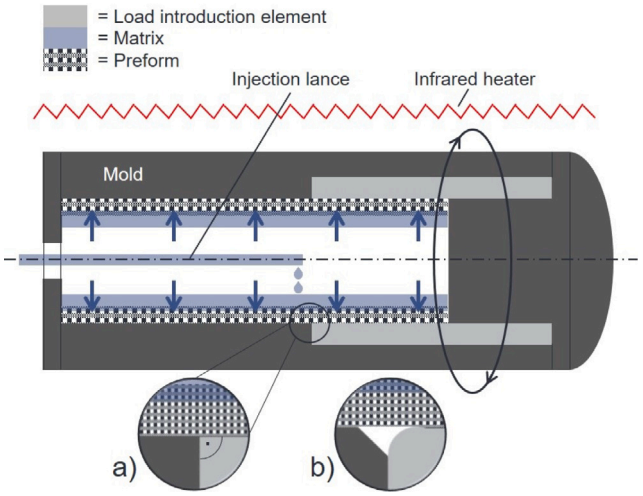

Fig. 1. Rotational molding process with a thermoset matrix [5,6].

for the joint strength of intrinsic hybrid composites [11,12]. Furthermore, it is known that small changes in the geometry of the joint can significantly influence the strength and failure of the joint. Analytical models show that the maximum stresses that cause failure occur at the ends of the overlap joint [13,14]. To reduce the stress concentration at the end of the overlap and increase the strength of the joint, spew fillets as well as reverse tapering or rounding of the adherend corners are proposed [15–28]. Adam et al. [15,16] investigated numerically and experimentally the effect of adhesive spew fillets and rounded adherend corners for both single-lap joints (SLJs) and double-lap joints (DLJs). They observed that the joint strength significantly increases in contrast to joints without spew fillet and rounded adherends. In addition, Adams and Peppiatt [29] also studied bonded tubular lap joints with spew fillets. However, they did not consider the influence of tapering or rounding the adherend corners. Hildebrand [17] conducted similar studies on SLJs made of fiber-reinforced plastic (FRP) and metal. Fifteen different shapes of the joint ends were investigated with nonlinear analyses. The most suitable shapes increased the joint strength by 90–150%. In contrast to Adam et al. Hildebrand also considered a denting of the adherend in order to decrease the stiffness locally. This should shift some of the stresses from the edge of the joint to the center of the joint. Tsai and Morton [18] used Moire interferometry to measure the deformation at the end of the adherend corner with and without spew fillet. In comparison to other studies, Lang and Mallick [19] concentrated on the geometry of spew fillets, and also investigated rounded fillets. Frostig et al. [20] developed and validated a closed-form high-order theory that shows the reduction of stress concentration when using spew fillets twice the thickness of the adhesive layer. Since the effect of the spew fillet angle has often been neglected, Belingardi [23] addressed this issue and determined the optimum angle for steel FRP SLJs, which is at about 45°. In order to obtain the ideal shape at the end of the joint with optimization methods, various approaches were developed by Rispler et al. [21] and Ejaz et al. [26]. Apalak and Engin [22] as well as Zhao et al. [27,28] investigate the initiation and propagation of damage at the adherend corners. The experimental results indicate that rounding the adhesive corner proves to be advantageous only with brittle adhesives and not with ductile ones. Deng and Lee [25] transferred the findings on lap joints to bondings with CFRP plates. Their research suggests that the effect of spew fillets at CFRP plates is significantly minor than for lap joints. Da Silva et al. [24] investigated CFRP-titanium DLJs at low temperatures. They conclude that using the composite as the outer adherend is beneficial for increasing joint strength. However, most approaches concentrate on the conventional adhesive bonding of SLJs and DLS, while no emphasis has so far been placed on co-cured tubular joints with spew fillets and rounded adherend corners. In addition, the influence of cooling from the process temperature to room has not yet been investigated for co-cured joints with shape-optimized overlap ends. This work thus pursues the objective of implementing a model for calculating the stress distribution in the adhesive layer of tubular CFRP-metal components manufactured by rotational molding. For this purpose, finite element analysis (FEA) is applied to examine the influence of spew fillets and the effect resulting from rounding the adherend corners. To this end, a design of experiment (DoE) is implemented, which also takes the cooling from process to room temperature into account. An optimized geometry with a reduced stress distribution at the end of the overlap is obtained and experimentally compared to a reference variant without spew fillet and rounded adherend corners.

Table 1
Summary of load cases.

Variable	Step	Magnitude
Temperature change	Cool down	80 K
Tensile force	Loading step	75 kN

2. Model design

In this chapter, the FE model is presented as well as the geometry used, the load cases, the material properties, and design parameters of the spew fillet.

2.1. Geometry

As shown in Fig. 2, the tie rod consists of a body made of CFRP with a thickness $t_c = 2$ mm and an aluminum load introduction element with a thickness $t_l = 3$ mm. Between the two parts, the co-cured joint was modeled with a very thin adhesive layer thickness $t_a = 0.1$ mm and an overlap length $l_o = 30$ mm. The inner radius of the load introduction element r_i was 20 mm. In order to limit the required calculation time, rotational symmetry around the central axis was used. Furthermore, instead of a conventional composite tie rod with two load introduction elements, only the overlap between one metallic load introduction element and the CFRP profile was considered (see Fig. 2).

2.2. Load cases

Since the tie rod is to be subjected to a tensile load, a constraint was implemented at the upper end of the metallic load introduction element to a reference point to which an axial tensile force was applied (see Fig. 2 and Table 1). The laminate was fixed at the lower end. During the rotational molding process, the heated matrix is introduced to the heated mold through an injection unit to impregnate the dry fiber preform. After the curing and demolding of the component, the composite tie rod cools down to room temperature. This change in temperature will lead to internal stresses which have to be considered. A temperature change of 80 K was thus assumed in the model before the loading step, which corresponds to the difference between process and room temperature.

2.3. Ply layup and fiber orientation

Due to the cooling from process temperature to room temperature, the different thermal expansion coefficients of aluminum and CFRP are of particular importance. While the thermal expansion of aluminum and matrix is isotropic, the thermal expansion of CFRP significantly depends on fiber orientation. This context is illustrated in Fig. 3, which shows the coefficient of thermal expansion α in transverse direction, which is crucial for the elongation of thin tubes. If the component is loaded in axial tensile direction, a high fiber content should be

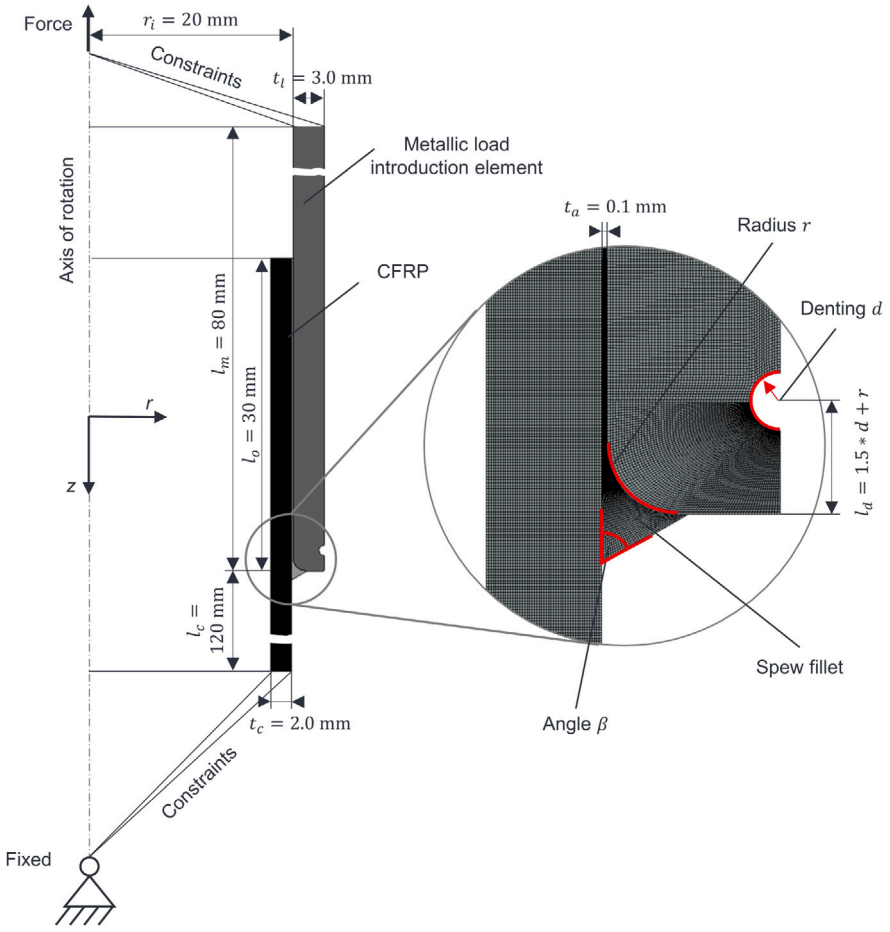

Fig. 2. Model of the composite tie rod with spew field and rounded corners of the aluminum load introduction element.

Table 2
Composite layup for Variant 1 (V1) and Variant 2 (V2).

Ply layup	Orientation and number of filaments
Variant 1 (V1)	$\pm 60°_{3K}$ /$\pm 60°_{3K}$/ $\pm 30°_{6K}$
Variant 2 (V2)	$\pm 60°_{3K}$ /$\pm 15°_{6K}$/ $\pm 15°_{6K}$

oriented in 0°-direction (y-direction, Fig. 2) to ensure high component stiffness in this direction. For the given component configuration, however, this would result in a stronger thermal contraction of the CFRP body compared to the one of the aluminum load introduction element when cooling down from process temperature, because the coefficient of thermal expansion of CFRP is higher than the one of aluminum at 0° (see Fig. 3). This would lead to a state which provokes damaging tensile stresses within the adhesive layer. To avoid tensile stresses in the adhesive layer and instead achieve stronger thermal contraction of the load introduction element compared to the laminate, fiber orientations with an angle of ± 60° were also applied in the present study. In order to better evaluate the influence of the fiber orientation, two different ply layups, Variant 1 (V1) and Variant 2 (V2), were defined (see Table 2). The use of braided carbon fiber sleeves limits the fiber orientation between ± 15°–70°. In both present variants, cooling induces a compressive stress in the adhesive layer. The difference between V1 and V2 consists in V1 causing more compressive stress in the adhesive layer, while V2 is characterized by a higher axial stiffness of the laminate. According to VDI 2014 [30], the ± layers were modeled in a simplified way by using thin UD-plies with + and - direction.

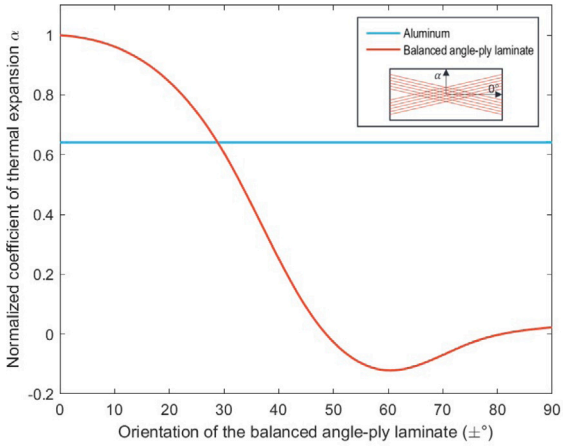

Fig. 3. Coefficients of thermal expansion α for CFRP and aluminum as a function of orientation [31].

2.4. Material properties

The FE model consisted of the three separate parts: Load introduction element, CFRP body and adhesive layer, for which different material models had to be applied. To reduce the total mass of the tie rod, the load introduction element was made of aluminum. The aluminum was modeled as linear elastic and a constant coefficient of thermal expansion was specified (see Table 3). For the matrix system of the CFRP, the epoxy *SR8500/SZ8525* from *Sicomin* [32] was used.

Table 3
Material properties from [31] and [32].

	E (N/mm^2)	ν	α (1/K)
Aluminum	70000	0.35	2.3E−05
Epoxy	3150	0.35	6.7E−5

Table 4
Material properties from [33].

Variable	Value	Unit
E_1	133860	N/mm^2
E_2	7706	N/mm^2
E_3	7706	N/mm^2
G_{12}	4306	N/mm^2
G_{13}	4306	N/mm^2
G_{23}	2760	N/mm^2
ν_{12}	0.301	
ν_{13}	0.301	
ν_{23}	0.396	
α_{11}	3.2E−7	1/K
α_{22}	2.6E−5	1/K
α_{33}	2.6E−5	1/K

Since the thin adhesive layer consists of pure matrix, the properties of the epoxy *SR8500/SZ8525* were chosen (see Table 3). The orientations were specified due to the orthotropic properties of the CFRP. The laminate was also based on linear elastic behavior and used mechanical properties are given in Table 4.

2.5. FE method

The numerical model was built using the *Dassault Systèmes Simulia* finite element software *Abaqus 2019*. It consisted of three key parts: the rotationally molded CFRP, the load introduction element and the connective adhesive layer in between (see Fig. 2). Since the Abaqus features – e.g. cohesive surface or cohesive elements – do not allow the modeling of geometrically complex spew fillets, a material model was implemented for the adhesive layer (see Section 2.4) and the surfaces were connected to CFRP and load introduction element via a tie constraint. This constraint links the cohesive layer to the CFRP and the load introduction element at the respective sides. The discretization for adhesive layer and load introduction element was performed using four node axisymmetric quadrilateral elements with reduced integration (element CAX4R). A four node axisymmetric quadrilateral element (CGAX4R) was also selected for the CFRP in order to be able to model anisotropic behavior. The size of the elements was determined on the basis of a convergence study and an analysis of the change in stresses (shear stress and maximum principal stresses) for a given specific mesh size. As the stresses converges with a mesh size below 1 mm, the FE model can be considered convergent. Hence, a mesh size of 0.1 mm was specified for a compromise of high accuracy and acceptable calculation time. The failure of the modeled component is expected to occur within the adhesive layer at the end of the overlap, where the spew fillet is located (see Fig. 2). Therefore, the boundary stresses were extracted in the analysis to identify potential failure regions. The stresses considered were peel, shear, longitudinal and maximum principal stresses.

2.5.1. Design parameters

For the purpose of designing a spew fillet in a way that minimizes stress peaks in the adhesive layer, design parameters were respectively defined and varied during the study. According to the state of the art (see Section 1), the following three parameters with the greatest influence were selected:

- Radius of the rounded load introduction element r
- Angle of the spew fillet β
- Denting of the load introduction element d

Table 5
Optimization limits for Isight.

Parameter	Minimum	Maximum
Radius r	0.1 mm	2 mm
Angle β	35°	80°
Denting d	0 mm	0.8 mm

The distance between the end of the metallic load introduction element and the center of the denting is determined by a formula (see Fig. 2), so that with a smaller denting d and a smaller radius r, the distance is also reduced. However, due to the given rotational molding process, not every parameter can be flexibly varied. The thickness of the adhesive layer t_a was kept constant since it is predetermined by the manufacturing process. Furthermore, the angle of the spew fillet β was limited to the range between 35° and 80°, because if the angle is too large, the centrifugal pressure could press the dry preform into the cavity (see Fig. 1 b) and the positive effect of the spew fillet would be lost. The design limits of each parameter are presented in Table 5.

2.6. Design of experiments

Dassault Systèmes Simulia Isight 2019 optimization framework was used for the automated variation of the selected design parameters and analysis of stresses. The procedure implemented in *Isight* can be described as follows:

- Abaqus: Conduct an analysis with predefined starting parameters
- Isight: Read in output from Abaqus
- Python script: Calculate cost function from stresses (see Section 2.6.1)
- Isight: Determine new parameters
- Abaqus: Update the model with the *Isight* parameters and repeat the process

A DoE was used to determine the parameter sets of each iteration. The cost function was calculated by a Python script (here: the maximum principal stresses of the adhesive layer, see Section 2.6.1) The optimization framework was selected for determining the relationship between stresses and geometry. Thus, an optimized set of parameters could be derived for the composite tie rod configuration. To determine sample parameters, the Latin hypercube technique proposed in [34] was used as it ensures good space filling properties whilst ensuring a high flexibility. Isight's Latin hypercube implementation was used throughout this process.

2.6.1. Definition of cost function

The objective of the DoE was to identify the dependence of the maximum stresses on the design parameters in order to reduce the stresses and ensure increased load capacity. To analyze the stresses for each parameter set, a Python script was used to extract the highest maximum principal stresses at the integration points within the adhesive layer. The maximum principal stresses were selected because they are primarily responsible for joint failure according to [28]. A cost function was calculated, which includes the stresses at N integration points. In order only to consider areas with high stresses, the 2% of integration points with the highest amount were selected. The maximum principal stresses at these integration points were normed by the volume corresponding to the integration point. This approach is similar to the approach of Katz et al. [2], however, by norming the cost by V_N, the physical interpretation of the cost is more explicit and less dependent on the magnitudes of the integration point volumes, which otherwise need to be factored in.

$$\mathcal{L} = \frac{1}{V_N} \sum_{n=1}^{N} \sigma_n v_n \tag{1}$$

Table 6
Compressive stresses within the adhesive layer and length changes of the component for a reference geometry without spew fillet.

Variant	Compressive stresses $\sigma_{rr,mean}$ (MPa)	Length changes Δz (mm)
V1	−6.51	1.01
V2	−1.98	0.41

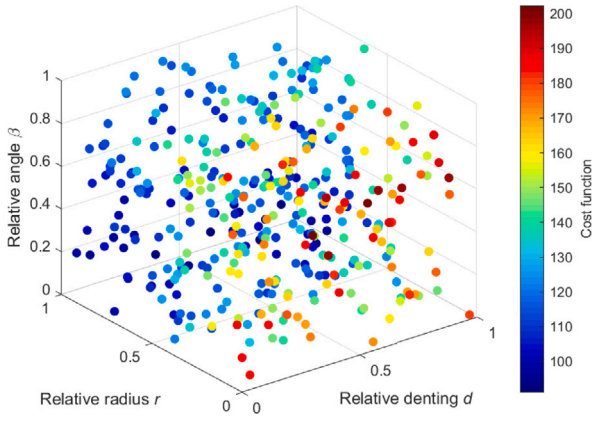

Fig. 4. Relative parameter space and results of the DoE for V1.

$$V_N = \sum_{n=1}^{N} v_n \tag{2}$$

$\mathcal{L}$: Cost function
σ_n : Sorted array of principal stresses at all integration points
N : Number of relevant integration points
V_N : Total volume of the N relevant integration points
v_n : Array of integration point volumes

3. Results

3.1. Numerical results

First, an analysis of the ply layup of V1 and V2 was carried out. The σ_{rr} stresses within the adhesive layer due to cooling and the length changes Δz of the components due to the applied force were compared on a model without a spew fillet (see Table 6). As expected (see Section 2.3) V1 shows higher compressive stresses within the adhesive layer, but V2 is axially stiffer and therefore stretches less.

A total of 800 simulations were performed for the DoE, each with 400 iterations for V1 and 400 iterations for V2. The relative parameter space related to the parameter limits of radius r, angle β and denting d is depicted in a three-dimensional graph in Figs. 4 and 5. The colors in the graph indicate the magnitude of the cost function, which shows that the radius r of the load introduction element and also the angle β of the spew fillet have a major impact on the maximum principal stresses. Furthermore, it can be seen that in general the magnitude of the cost function of V1 is much higher (value range 90–200) than the magnitude of V2 (value range 65–125). As a result, it can be deduced that V1 withstands a lower tensile load than V2. Consequently, the higher axial stiffness of V2 has a more significant positive influence on the stress levels than the higher thermally induced compressive stresses in V1.

The plot in Figs. 6 and 7 also proves a dependence of the cost function on the radius r and angle β. The quadratic regressions of the stresses and the parameters indicate that the radius r of the load introduction element should be chosen as large as possible, whereas the angle of the spew fillet β should be chosen as small as possible. The denting only has a very minor influence on the cost function, therefore no regression was calculated. A detailed list of the correlation factors for V1 and V2 can be found in Table 7. Overall, the correlation for

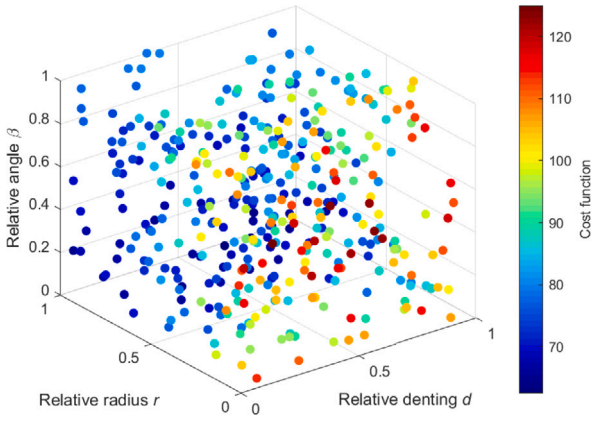

Fig. 5. Relative parameter space and results of the DoE for V2.

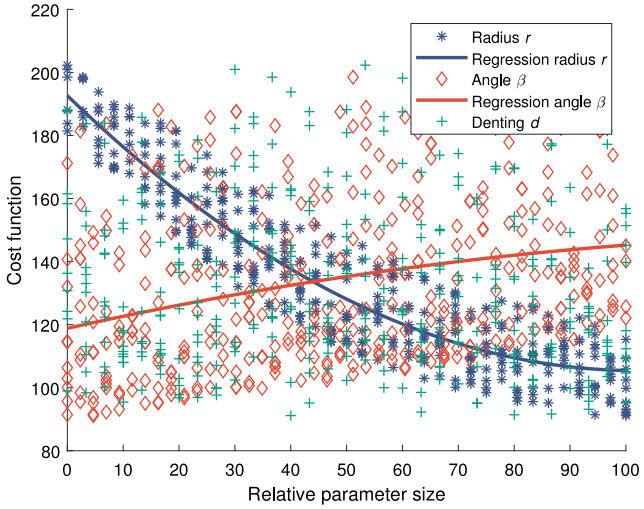

Fig. 6. Results of DoE with calculation of quadratic regressions for V1.

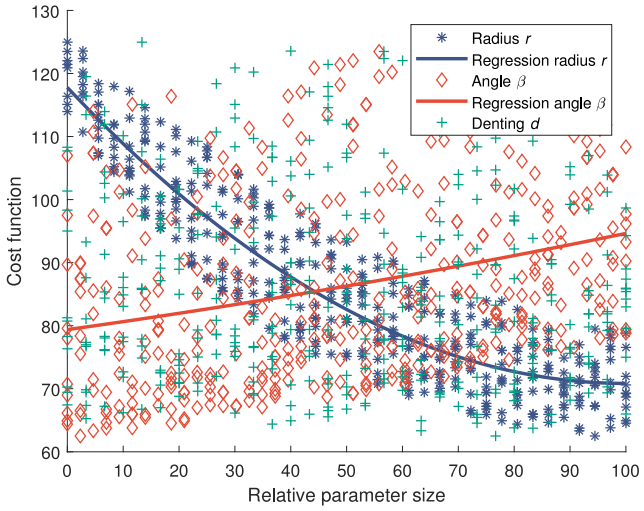

Fig. 7. Results of DoE with calculation of quadratic regressions for V2.

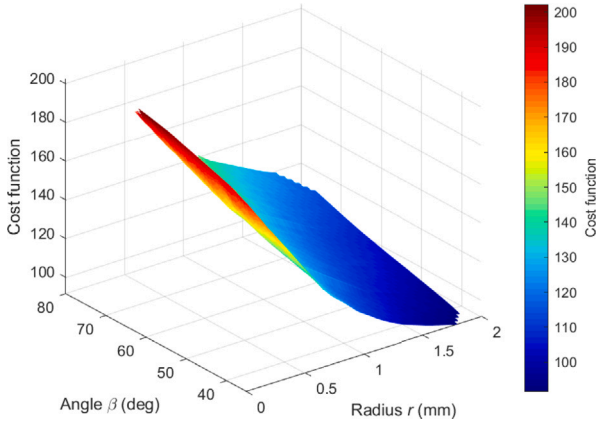

Fig. 8. Comparison of the influence of angle and radius for V1.

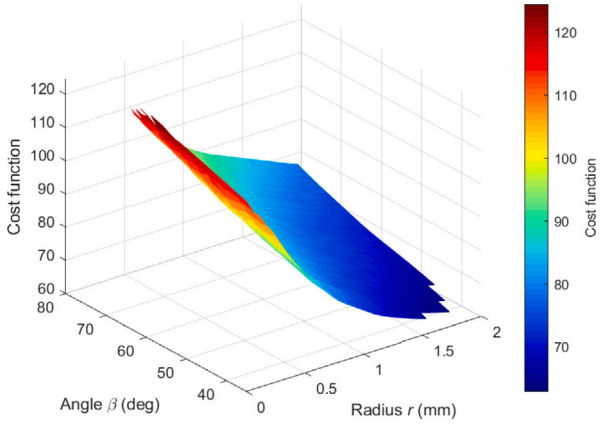

Fig. 9. Comparison of the influence of angle and radius for V2.

Table 7
Correlation coefficient R between the cost function and the design parameters for V1 and V2.

Variant	Correlation R radius r	Correlation R angle β	Correlation R denting d
V1	0.96	0.29	0.10
V2	0.92	0.30	0.07

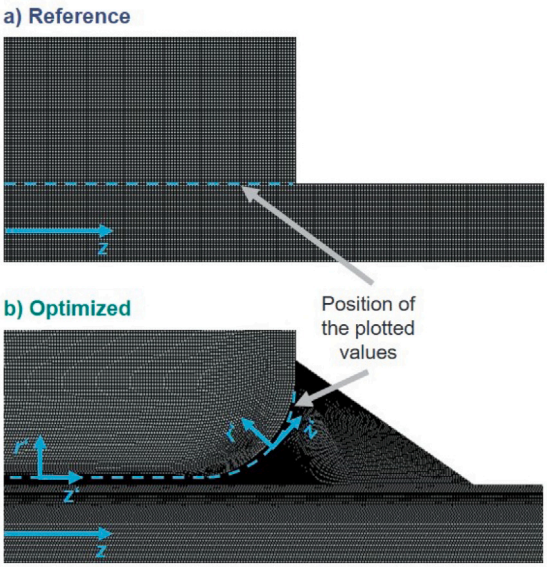

Fig. 10. Position of the plotted values for optimized and reference geometry.

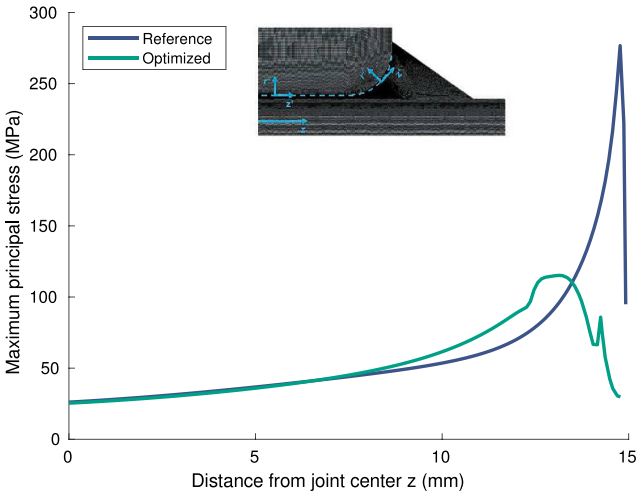

Fig. 11. Maximum principal stresses within the adhesive layer for V1.

the radius r and the highest maximum principal stresses was higher (R = 0.96 for V1 and R = 0.92 for V2) than the correlation between the angle β and the stress (R = 0.29 for V1 and R = 0.3 for V2). This implies that a change in radius r has a stronger impact on the stress level, which is also evident in Figs. 8 and 9, where the slope is largest with radius changes. As the angle β decreases, the cost function also decreases. However, this correlation is weaker. Furthermore, the correlation factors show that the denting d has hardly any influence (R = 0.10 for version 1 and R = 0.07 for V2). In contrast to Hildebrand [17], the numerical results do not indicate that denting shifts the critical stresses from the end to the middle of the joint, thus increasing the joint strength. Due to the very clear results of the DoE, the use of an optimization algorithm was omitted. The smallest angle and the largest radius were chosen for the experimental investigations (see Table 8). Since the denting does not have any impact on the stresses, it was removed to avoid a further process step and thus higher manufacturing costs. In the following, this design parameter set is referred to as optimized. The calculated stresses are plotted in Figs. 11–17 to allow a more profound understanding of the stresses within the adhesive layer at the end of the overlap. The optimized parameter set derived from the DoE is compared with a reference for V1 and V2. In contrast to the optimized variant, the reference does not have a spew fillet or a rounding of the metallic load introduction element, but a sharp corner at the end of the overlap with a 90° angle, identical to the one shown in Fig. 1 a). Fig. 10 shows the location of the plotted values for reference and optimized geometry. In order to obtain pure peel $\sigma_{r'r'}$ and shear stresses $\sigma_{r'z'}$, also for the optimized geometry at the critical curved part of the adhesive layer, the local coordinate system was chosen, which is tangentially aligned to the curve (see Fig. 10 b). Fig. 11 and Fig. 13 show the curves for the maximum principal stresses for V1 and V2. In the middle area of the overlap, almost no difference can be noticed between optimized shape and reference geometry. At the end of the overlap, however, the advantages of spew fillet and rounding of the load introduction element become evident. The maximum principal stress curves demonstrate a stress singularity for the reference geometry at the end of the overlap. In contrast, the highest stresses of the optimized shapes with spew fillet and rounded load introduction element are significantly lower. This can also be seen from the contour plot of the maximum principal stresses in Fig. 12. The spew fillet shifts the area with the highest stresses more to the center of the joint. Compared to the reference, the maximum principal stress

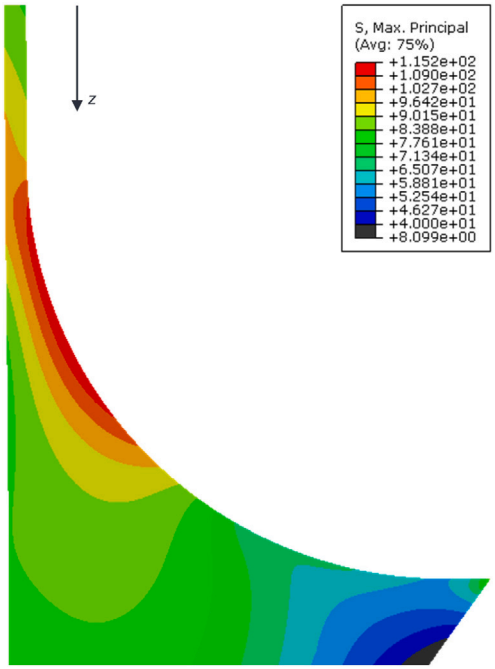

Fig. 12. Contour plot of the critical area of the adhesive layer for the optimized geometry of variant V1 with maximum principal stresses.

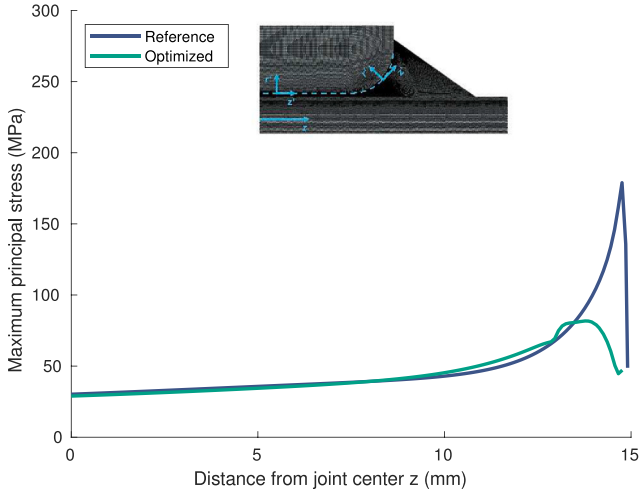

Fig. 13. Maximum principal stresses within the adhesive layer for V2.

Table 8
Selected design parameters for experimental investigations according to DoE.

Design parameter	Value
Radius r	2 mm
Angle β	35°
Denting d	0 mm

curves increase slightly earlier and fall again before the edge of the joint. The occurrence of the second peak in Fig. 11 can be explained with the stress distribution from Fig. 12. In Figs. 14 and 15 stress curves for the harmful peel stresses $\sigma_{r'r'}$ are shown. Also these evaluations show that with the spew fillet the maximum stresses can be reduced and the critical zone shifts more to the center of the joint. The same applies to the shear stress curves shown in Figs. 16 and 17.

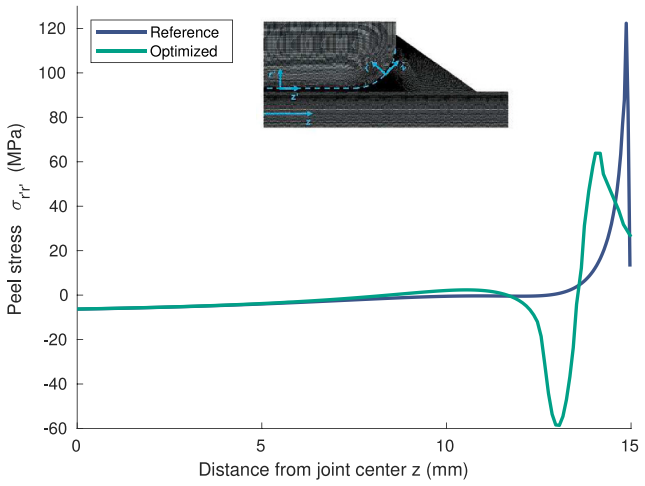

Fig. 14. Peel stresses ($\sigma_{r'r'}$) within the adhesive layer for V1.

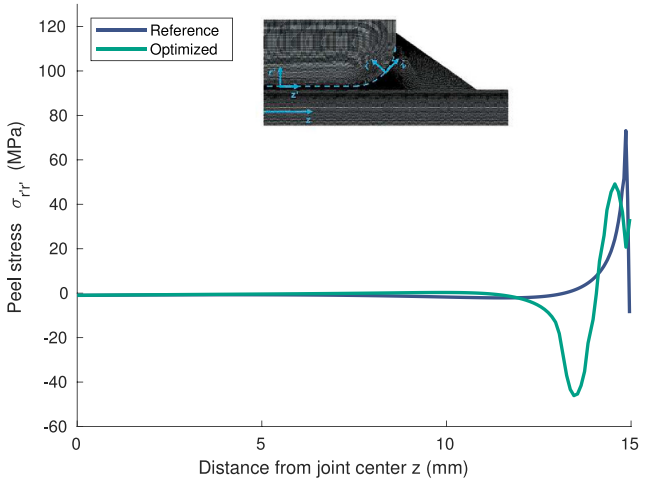

Fig. 15. Peel stresses ($\sigma_{r'r'}$) within the adhesive layer for V2.

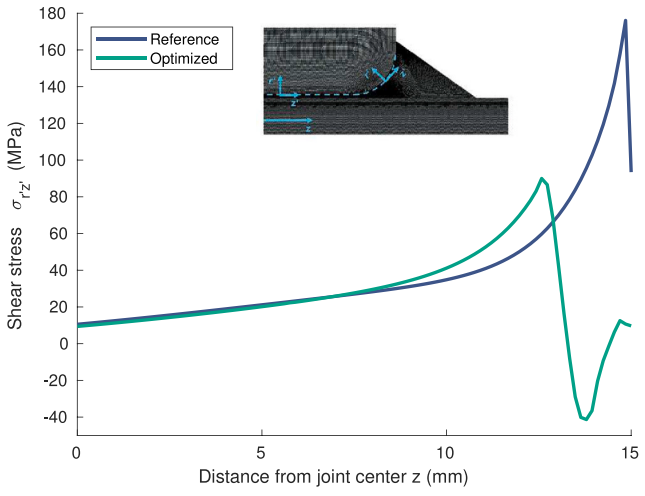

Fig. 16. Shear stresses ($\sigma_{r'z'}$) within the adhesive layer for V1.

V2 also shows an advantage over V1 for the maximum principal, peel and shear stress curves, as can be seen in the previous figures and in particular in the cost function. It can thus be assumed that V2

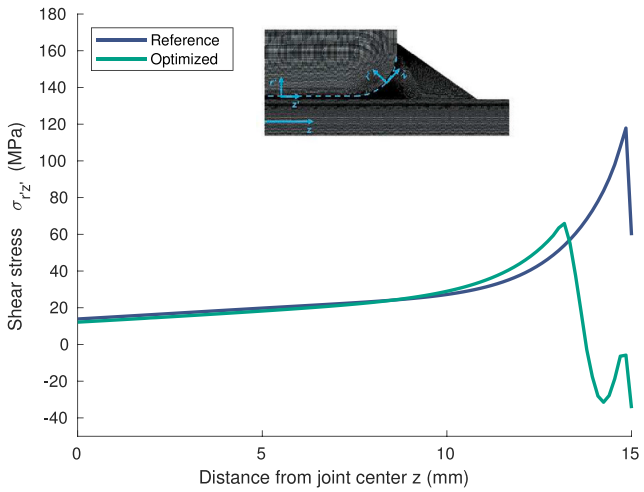

Fig. 17. Shear stresses ($\sigma_{r'z'}$) within the adhesive layer for V2.

withstands a higher tensile force. However, the absolute reduction of maximum principal, peel ($\sigma_{r'r'}$) and shear stresses ($\sigma_{r'z'}$) from reference to optimized geometry is higher for V1.

3.2. Experimental investigations

3.2.1. Test setup

The numerical results demonstrate that an adhesive spew fillet and rounded corners of the aluminum load introduction element can reduce the stresses within the adhesive layer and thus increase the joint strength of the rotationally molded composite tie rod. As with all FE modeling, certain simplifications had to be made for this purpose. Experimental investigations were therefore conducted to validate the numerical results. A total of sixteen specimens were produced by rotational molding (see Table 9). These sixteen specimens consisted of eight specimens from V1 and eight specimens from V2. Four specimens with optimized geometry and four reference specimens were produced for each variant. The specimens with optimized geometry had a spew

Table 9
Specimen Overview.

Specimen	Quantity	Radius r	Angle β
Optimized V1	4	2 mm	35°
Reference V1	4	–	90°
Optimized V2	4	2 mm	35°
Reference V2	4	–	90°

fillet with a 2 mm rounded corner of the aluminum adherend and a 35° angle (see Fig. 18). Based on the numerical results, the angle β may be chosen even larger. Limiting the angle to 35° pursued the objective of preventing the dry semi-finished fiber products from being pressed into the spew fillet during rotational molding and thus impeding the beneficial effect of the geometry. As defined in Section 3.1, the reference specimens did not have a spew fillet, thus, there was a sharp corner with a 90° angle at the end of the overlap. Therefore, two different tool molds were required to produce the specimens.

In order to increase the adhesive strength of the intrinsic interface, the surfaces of the aluminum load introduction elements were sandblasted with corundum. This results in a rough surface with a R_a of 3.2 µm. Braided sleeves of carbon fibers were used for the composite layup (see Table 2) of V1 and V2. These were layerwise applied with a thermoplastic binder powder to ensure safe handling when placing them into the mold and to prevent the preform from collapsing. The sealed mold with the carbon fiber preform and the load introduction element was then preheated in an oven at 100 °C for one hour. The tool was subsequently clamped in a lathe and rotated at 3000 rpm. During rotation, the blackened mold was further heated with infrared radiators to maintain a temperature of 100 °C, and the thermoset matrix was injected through the open mold side. To ensure complete curing, the specimens were rotated for 20 min and exposed to a downstream tempering cycle in the following. Afterwards, specimens were tested quasi-statically with a *Zwick* testing machine following DIN EN 1465 [35].

3.2.2. Experimental results

V1 shows a significant advantage of the optimized geometry compared to the reference, as can be seen in Fig. 19. The average maximum joint strength of the optimized geometry related to the overlap area

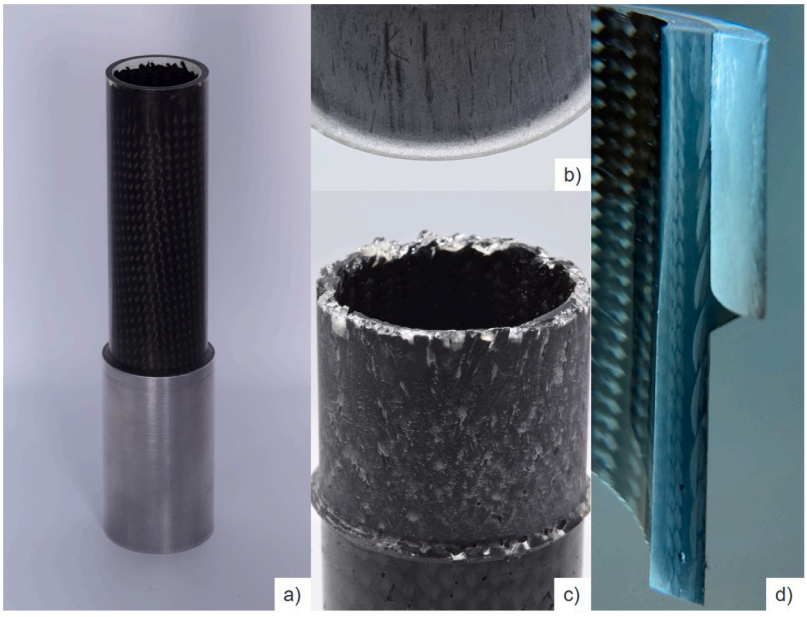

Fig. 18. (a) Rotationally molded composite tie rod specimen with spew fillet and rounded load introduction element, (b) Surface of the tested load introduction element including the rounding, (c) CFRP surface after joint failure, (d) Cross-section surface of the undamaged part.

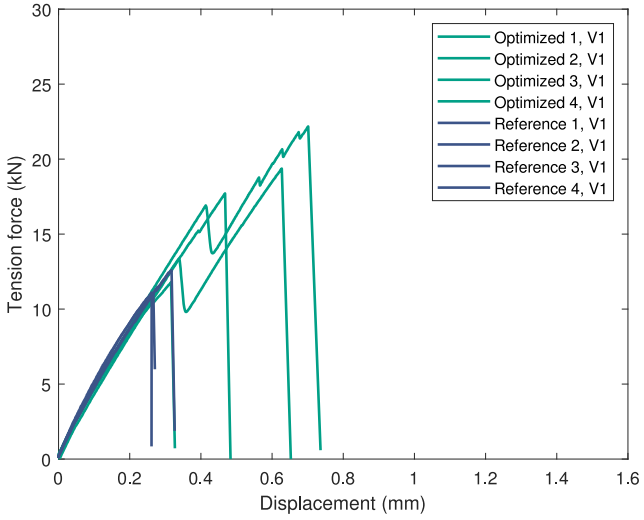

Fig. 19. Force displacement curve for V1.

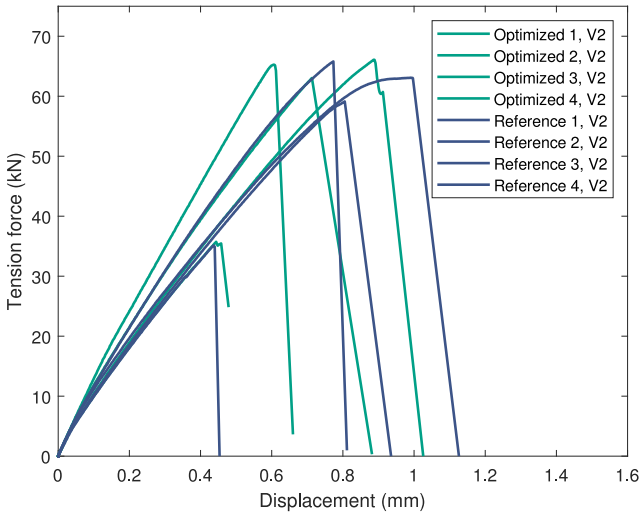

Fig. 20. Force displacement curve for V2.

amounts to 4.8 N/mm^2, whereas the average maximum joint strength for the reference only measures 3.1 N/mm^2 as shown in Fig. 21. It can be noted that the specimens with optimized shape often experience an initial failure, but the force can then be further increased up to the maximum failure (see Fig. 19). V2 generally shows higher maximum joint strength with 14.8 N/mm^2 for the reference specimen and 15.3 N/mm^2 for the specimen with optimized geometry (see Figs. 20 and 22). The best specimens withstand a tensile force of up to 65 kN. As expected from the numerical results, the effect of the spew fillet is less significant for V2 than for V1, however, V2 has the higher maximum tensile strength due to its high axial stiffness. In this respect, the experimental results confirm the numerical investigations. Overall, the experimental results show some scatter, which may be attributed to the low degree of automation. In addition, the effect of the spew fillet is slightly lower than expected from the results of the numerical calculation. All specimens failed mainly adhesively in the adhesive layer on the side of the metallic load introduction element as can be seen in Fig. 18. Only individual fibers and a small amount of matrix remain on the side of the load introduction element. The complete spew fillet of matrix remains on the side of the CFRP body at failure and only a few smaller particles break out of the surface and stick to the load introduction element. It can be observed from the cross-section surface of the undamaged part in Fig. 18, that no fibers of the preform were pressed into the spew fillet during rotational molding. In future designs, it might thus be possible to opt for an even larger radius r of the rounding and an even smaller angle β of the spew fillet.

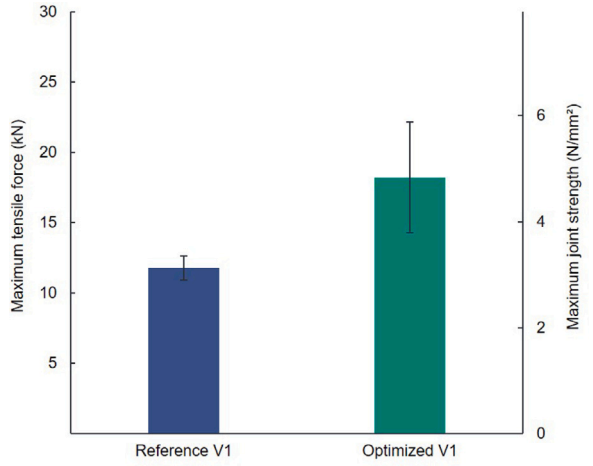

Fig. 21. Joint strength and maximum tensile force with calculated standard deviation for V1.

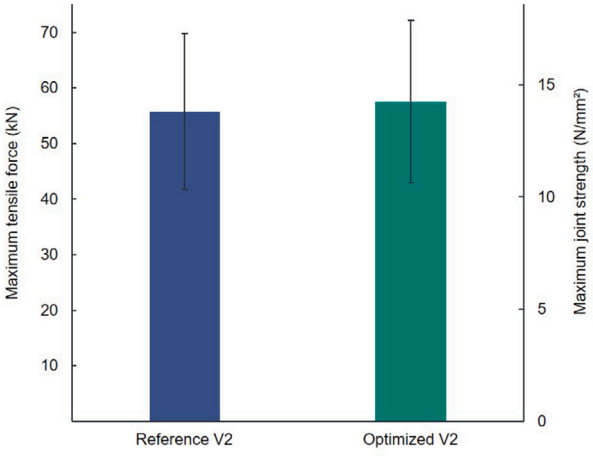

Fig. 22. Joint strength and maximum tensile force with calculated standard deviation for V2.

4. Conclusion

This paper pursued the objective of investigating the influence of spew fillets with rounded adherend corners to improve the joint strength of a rotationally molded composite tie rod. For this purpose, a parametric FE model was implemented, and a DoE was selected to individually investigate the influence of different geometry parameters of the spew fillet. The numerically results were compared to tensile tests of rotationally molded specimens. According to the numerical analyses and the experimental investigations, the following conclusions were drawn:

- The experimental results indicate that the rotational molding process can be used for producing hybrid components with high strength and low cycle times. Compared to conventional manufacturing processes, the laminate and load introduction elements do not have to be subsequently joined.

- Spew fillets with rounded adherend corners can be used for reducing the stresses in the adhesive layer of rotationally molded components and increase joint strengths. The effort required for implementing a spew fillet is extremely low and only needs to be considered when machining the mold and load introduction element.
- Increasing the radius of the adherend corner has a particularly positive effect on the joint strength. The angle of the spew fillet should be selected as small as possible. However, no increase in joint strength can be achieved with denting, according to numerical studies.
- To achieve high joint strength, the fibers in the laminate should be axially oriented, as this ensures high axial stiffness. Although an orientation in circumferential direction increases the compressive stresses in the adhesive layer when the process temperature cools to room temperature, this effect does not contribute as significantly to the increase in strength as the high stiffness caused by axially oriented fibers. However, the advantages of rounded adherend corners and spew fillets are reduced with increasing axial stiffness.

Funding source

This project was funded by the German Research Foundation (DFG: Deutsche Forschungsgemeinschaft). It formed part of the collaborative research priority program 1712: “Intrinsic hybrid composites for lightweight structures”.

CRediT authorship contribution statement

Jonas Nieschlag: Conceptualization, Methodology, Software, Writing – original draft. **Philipp Eisenhardt:** Formal analysis, Data curation, Visualization. **Sven Coutandin:** Writing – review & editing. **Jürgen Fleischer:** Supervision, Writing – review & editing, Funding acquisition.

Declaration of competing interest

The authors declare that they have no known competing financial interests or personal relationships that could have appeared to influence the work reported in this paper.

Acknowledgments

The authors wish to thank Tayfun Murat and Ralf Sturm for their support during production and test execution. Furthermore, the authors wish to express their gratitude to Siltex Flecht- und Isoliertechnologie Holzmüller GmbH & Co.KG for providing the braided sleeves and the Institute for Applied Materials (KIT) for granting the opportunity of using their testing machines.

References

[1] Jegley DC, Wu KC, Phelps JE, McKenney MJ, Oremont L. Structural efficiency of composite struts for aerospace applications. J Spacecr Rockets 2012;49:915–24. http://dx.doi.org/10.2514/1.A32085.

[2] Katz J, Klimach M, Haupt F, Brechtel A, Mittelstedt C. Structural optimization and experimental investigation of CFRP lock nuts. Composites A 2019;117:156–68. http://dx.doi.org/10.1016/j.compositesa.2018.11.004.

[3] Fleischer J, Teti R, Lanza G, Mativenga P, Möhring H-C, Caggiano A. Composite materials parts manufacturing. CIRP Annal 2018;67:603–26. http://dx.doi.org/10.1016/j.cirp.2018.05.005.

[4] Ehleben M, Schürmann H. Manufacturing of centrifuged continuous fibre-reinforced precision pipes with thermoplastic matrix. Compos Sci Technol 2006;66:2601–9. http://dx.doi.org/10.1016/j.compscitech.2006.03.015.

[5] Fleischer J, Koch S-F, Coutandin S. Manufacturing of polygon fiber reinforced plastic profiles by rotational molding and intrinsic hybridization. Prod Eng 2015;9:317–28. http://dx.doi.org/10.1007/s11740-015-0620-0.

[6] Koch SF, Barfuss D, Bobbert M, Groß L, Grützner R, Riemer M, Stefaniak D, Wang Z. Intrinsic hybrid composites for lightweight structures: new process chain approaches. In: Advanced materials research, Trans Tech Publ: p. 239–46. http://dx.doi.org/10.4028/www.scientific.net/AMR.1140.239.

[7] Koch S-F, Peter M, Fleischer J. Lightweight design and manufacturing of composites for high-performance electric motors. Procedia CIRP 2017;66:283–8. http://dx.doi.org/10.1016/j.procir.2017.03.274.

[8] Nieschlag J, Coutandin S, Fleischer J. Production and tensile testing of rotationally molded hybrid composite tie rods. In: SAMPE 2020 virtual series—multifunctional materials and structures. 2020, URL https://www.nasampe.org/store/viewproduct.aspx?id=16320936.

[9] Pocius AV. Adhesion and adhesives technology: an introduction. Carl Hanser Verlag GmbH Co KG; 2021, http://dx.doi.org/10.3139/9783446431775.

[10] Page SA, Berg JC, Månson J-A. Characterization of epoxy resin surface energetics. J Adhes Sci Technol 2001;15:153–70. http://dx.doi.org/10.1163/156856101743382.

[11] Zinn C, Bobbert M, Dammann C, Wang Z, Tröster T, Mahnken R, Meschut G, Schaper M. Shear strength and failure behaviour of laser nano-structured and conventionally pre-treated interfaces in intrinsically manufactured CFRP-steel hybrids. Composites B 2018;151:173–85. http://dx.doi.org/10.1016/j.compositesb.2018.05.030.

[12] Gebhardt J, Fleischer J. Experimental investigation and performance enhancement of inserts in composite parts. Procedia CIRP 2014;23:7–12. http://dx.doi.org/10.1016/j.procir.2014.10.084.

[13] Volkersen O. Die nietkraftverteilung in zugbeanspruchten nietverbindungen mit konstanten laschenquerschnitten. Luftfahrtfor Schung 1938;15:41–7.

[14] Goland M, Reissner E. The stresses in cemented joints. J Appl Mech 1944;17:66.

[15] Adams RD, Atkins RW, Harris JA, Kinloch AJ. Stress analysis and failure properties of carbon-fibre-reinforced-plastic/steel double-lap joints. J Adhes 1986;20:29–53. http://dx.doi.org/10.1080/00218468608073238.

[16] Adams RD, Harris JA. The influence of local geometry on the strength of adhesive joints. Int J Adhes Adhes 1987;7:69–80. http://dx.doi.org/10.1016/0143-7496(87)90092-3.

[17] Hildebrand M. Non-linear analysis and optimization of adhesively bonded single lap joints between fibre-reinforced plastics and metals. Int J Adhes Adhes 1994;14:261–7. http://dx.doi.org/10.1016/0143-7496(94)90039-6.

[18] Tsai MY, Morton J. The effect of a spew fillet on adhesive stress distributions in laminated composite single-lap joints. Compos Struct 1995;32:123–31. http://dx.doi.org/10.1016/0263-8223(95)00059-3.

[19] Lang TP, Mallick PK. Effect of spew geometry on stresses in single lap adhesive joints. Int J Adhes Adhes 1998;18:167–77. http://dx.doi.org/10.1016/S0143-7496(97)00056-0.

[20] Frostig Y, Thomsen OT, Mortensen F. Analysis of adhesive-bonded joints, square-end, and spew-fillet—high-order theory approach. J Eng Mech 1999;125:1298–307. http://dx.doi.org/10.1061/(ASCE)0733-9399(1999)125:11(1298).

[21] Rispler AR, Tong L, Steven GP, Wisnom MR. Shape optimisation of adhesive fillets. Int J Adhes Adhes 2000;20:221–31. http://dx.doi.org/10.1016/S0143-7496(99)00047-0.

[22] Apalak MK, Engin A. Effect of adhesive free-end geometry on the initiation and propagation of damaged zones in adhesively bonded lap joints. J Adhes Sci Technol 2004;18:529–59. http://dx.doi.org/10.1163/156856104839293.

[23] Belingardi G, Goglio L, Tarditi A. Investigating the effect of spew and chamfer size on the stresses in metal/plastics adhesive joints. Int J Adhes Adhes 2002;22:273–82. http://dx.doi.org/10.1016/S0143-7496(02)00004-0.

[24] Da Silva LFM, Adams RD. Techniques to reduce the peel stresses in adhesive joints with composites. Int J Adhes Adhes 2007;27:227–35. http://dx.doi.org/10.1016/j.ijadhadh.2006.04.001.

[25] Deng J, Lee MMK. Effect of plate end and adhesive spew geometries on stresses in retrofitted beams bonded with a CFRP plate. Composites B 2008;39:731–9. http://dx.doi.org/10.1016/j.compositesb.2007.05.004.

[26] Ejaz H, Mubashar A, Ashcroft IA, Uddin E, Khan M. Topology optimisation of adhesive joints using non-parametric methods. Int J Adhes Adhes 2018;81:1–10. http://dx.doi.org/10.1016/j.ijadhadh.2017.11.003.

[27] Zhao X, Adams RD, Da Silva LF. Single lap joints with rounded adherend corners: experimental results and strength prediction. J Adhes Sci Technol 2011;25:837–56. http://dx.doi.org/10.1163/016942410X520880.

[28] Zhao X, Adams RD, Da Silva LF. Single lap joints with rounded adherend corners: stress and strain analysis. J Adhes Sci Technol 2011;25:819–36. http://dx.doi.org/10.1163/016942410X520871.

[29] Adams RD, Peppiatt NA. Stress analysis of adhesive bonded tubular lap joints. J Adhes 1977;9:1–18. http://dx.doi.org/10.1080/00218467708075095.

[30] VDI. Vdi 2014, part 3: Development of FRP components (fibre-reinforced plastics) - analysis. 2006, URL https://www.vdi.de/richtlinien/details/vdi-2014-blatt-3-development-of-fibre-reinforced-plastics-components-analysis.

[31] Schürmann H. Konstruieren Mit Faser-Kunststoff-Verbunden, vol. 2. Springer; 2005, http://dx.doi.org/10.1007/978-3-540-72190-1.

[32] Sicomin. Technical datasheet: SR 8500 / SZ 8525 fast and clear epoxy system for hot processes. 2021/01, URL http://www.sicomin.com/datasheets/product-pdf1158.pdf.

[33] Barbero EJ. Finite Element Analysis of Composite Materials using AbaqusTM. CRC Press; 2013, http://dx.doi.org/10.1201/b14788.

[34] McKay MD, Beckman RJ, Conover WJ. A comparison of three methods for selecting values of input variables in the analysis of output from a computer code. Technometrics 2000;42:55–61. http://dx.doi.org/10.1080/00401706.2000.10485979.

[35] DIN EN 1465. Adhesives - determination of tensile lap-shear strength of bonded assemblies. 2009-07, http://dx.doi.org/10.31030/1507601.